PAPER

Check for updates

A first-principles investigation of pressure induced topological phase transitions in half-Heusler AgSrBi

Bhautik R. Dhori, [iD] [a] Raghottam M. Sattigeri, [iD] [a] Prafulla K. Jha, [iD] *[a] Dominik Kurzydlowski [iD] [b] and Brahmananda Chakraborty [iD] [c]

Topological insulators (TI) are materials with novel quantum states and exhibit a bulk insulating gap, while their edge/surface is conducting. This has been extensively explored in several half-Heusler (HH) compounds. In the present work we employ first-principles calculations based on density functional theory to perform thorough investigations of pressure induced topological phase transitions (TPT) in HH AgSrBi which belongs to the $F\bar{4}3m$ space group. AgSrBi is intrinsically semi-metallic in nature which under isotropic pressure exhibits a semi-metal to trivial insulator transition while retaining the cubic symmetry. Also, we observe that this phase of AgSrBi is dynamically stable at extreme pressures as high as ~ 23.5 GPa. However, on breaking the cubic symmetry we observe the much desired TI nature after a non-trivial phase transition from a semi-metal to TI. We also explore the effect of lowering the crystal symmetry along with dimensional confinement in realizing a two-dimensional (2D) TI, AgSrBi, which is done by cleaving the [111] crystal plane. We perform a qualitative analysis of the electronic properties to understand the origin of this non-trivial behavior in the bulk and 2D phases of AgSrBi. This is accompanied by a quantitative analysis of the $\mathbb{Z}_2$ invariants and surface/edge state spectra, which further confirms the TI nature of AgSrBi. Hence, we propose the bulk as well as 2D phase of AgSrBi as a dynamically stable TI which can be used as ultra-thin films for thermoelectric, spintronic and nanoelectronic applications.

1 Introduction

The discovery of the quantum spin hall effect (QSHE)[1] and the governing topological properties of a material have sparked a lot of interest in the exotic and non-trivial phases of matter such as topological insulators (TI), Dirac semi-metals, nodal-line semimetals, *etc.*[2–7] Followed by the theoretical prediction, the experimental realization of such materials has opened up numerous avenues from the application point of view which is not just restricted to spintronics and quantum computations, but also extended to thermoelectricity, superconductivity, *etc.*[8–10] TI are essentially insulating in the D dimension and conducting in the D–1 dimension, *i.e.*, in a three-dimensional regime, the bulk is insulating but the surfaces are conducting in nature. This is by virtue of the time reversal symmetry which

makes these conducting surface states topologically robust against external perturbations. Such behavior was initially observed in the bulk quintuple layered system $Bi_{1-x}Sb_x$,[11,12] which was preceded by numerous other compounds with similar structures such as Bi_2Te_3, Sb_2Te_3,[13] *etc.* However, the search for such non-trivial topological properties was also conducted in other crystal structures such as binary compounds of group IV–VI compounds, magnetic compounds such as AMgBi (A = Li, Na, K)[14,15] and full- and half-Heusler (HH) compounds (which are also known for their thermoelectric, piezoelectric, magnetic and superconducting properties).[16–21]

The exciting possibility of multifunctional properties along with TI properties makes HH materials ideal candidates from the application point of view. HH compounds also exist in different polytypes such as hexagonal, orthorhombic, cubic, *etc.*[22] However, the cubic structure belonging to the $F\bar{4}3m$ space group is widely explored from the topological perspective since the zinc blende sub-lattice gives rise to band orders that are similar to those of HgTe because they are connected *via* topological adiabatic connection.[23] Also, the topological character in a typical HH ABC crystal arises due to the cation (A) substitution in the anion (BC) zinc blende sub-lattice. Hence,

[a] *Department of Physics, Faculty of Science, The Maharaja Sayajirao University of Baroda, Vadodara-390002, Gujarat, India. E-mail: prafullaj@yahoo.com*

[b] *Faculty of Mathematics and Natural Sciences, Cardinal Stefan Wyszyński University, ul. Wóycickiego 1/3, Warsaw 01-938, Poland*

[c] *High Pressure and Synchrotron Radiation Physics Division, Bhabha Atomic Research Centre, Trombay, Mumbai 40085, India*

HH compounds are potential candidates which can exhibit rich and diverse properties of interest.[16–21] However, not every HH compound exhibits the TI nature intrinsically as observed in Bi_2Te_3 and Sb_2Te_3[13] which arises due to the strong influence of spin–orbit coupling (SOC) between the core and valence electrons giving rise to relativistic effects; rather, HH compounds exhibit the TI character under different scenarios such as the influence of pressure/strain, electric field, doping, and vacancy and dimensional engineering.[24–29] These mechanisms have been explored in various HH compounds; however, HH compounds based on silver remain quite unexplored theoretically as well as experimentally leading to scarcity of data.

HH systems such as AgSrX with X = As, Sb, Bi have been predicted to be thermodynamically stable;[22] however, there is a lack of clarity on their electronic and topological properties, with AgSrAs[17] being an exception in this regard, since it has been explored for its structural and piezoelectric properties. AgSrBi displays some unconventional electronic properties with semi-metallic behavior. Although several materials have been predicted for their interesting topological properties with the help of machine learning techniques,[30,31] the HH system AgSrX (X = As, Sb, Bi) has not yet been predicted via such an effort. This inspired us to explore and thoroughly investigate AgSrBi in terms of the SOC interactions and their influence on the topological character. Thus, in the present study we explore the structural, electronic and topological properties of AgSrBi. We observe that the semi-metallic character of AgSrBi is retained even when SOC is considered. This motivated us to explore different potential routes to realise the non-trivial topological nature of AgSrBi. This is achieved by (i) breaking the cubic symmetry and (ii) lowering the crystal symmetry along with dimensional confinement along the [001] crystal direction (which gives rise to quantum confinement effects).[32–34] The former mechanism is known to lift off the degeneracy at the Fermi level, while the latter gives rise to quantum spin hall effects which bring about robust surface and edge states, respectively. With a focus on the topological character of AgSrBi, we perform a qualitative analysis of the electronic band structure, followed by a quantitative analysis of the $\mathbb{Z}_2$ topological class. We find that AgSrBi can exhibit non-trivial TI nature when the cubic symmetry is broken and the crystal symmetry is lowered to the hexagonal phase from the face centered cubic phase along with dimensional confinement along the [001] crystal direction. We further classify this with the $\mathbb{Z}_2$ invariant as $(\nu_0, \nu_1\nu_2\nu_3) = (1, 101)$ and $\nu = 1$ which indicates the strong and non-trivial TI nature, respectively. This suggests that the thin films of AgSrBi can be either exfoliated or synthesized by using techniques such as molecular beam epitaxy for applications in nanoelectronics and spintronics.[35,36]

2 Methodology

We use first-principles calculations based on density functional theory (DFT) implemented using the Quantum ESPRESSO code[37] to calculate and investigate the electronic properties of

AgSrBi. We use norm conserving pseudopotentials under generalized gradient approximation based on the Martins–Troullier method[38] with an exchange correlation energy functional of the Perdew–Burke–Ernzerhof type.[39] This pseudopotential considers $4d^{10}5s^1$, $5s^2$ and $6s^26p^3$ orbitals of As, Sr and Bi, respectively. In order to consider the relativistic effect of the core electrons on the valence electrons in SOC calculations, pseudopotential based on the projector augmented wave (PAW) method was used. The ground state of the system was optimized by following the bisection convergence method to locate the global minima with a convergence threshold of the order of $<10^{-8}$ Ry. A kinetic energy cutoff of 80 Ry was adopted for the basis set with the irreducible Brillouin zone (BZ) sampled on a uniform Monkhorst–Pack grid[40] k-mesh of $8 \times 8 \times 8$ and $8 \times 8 \times 1$. The vibrational properties were calculated using density functional perturbation theory (DFPT)[41] with a q-mesh of $6 \times 6 \times 6$ and $6 \times 6 \times 1$ for the bulk and low-dimensional phase, respectively. From the perspective of potential room temperature applications, we also performed ab initio molecular dynamics (AIMD) simulations for a time step of 3 picoseconds (3000 femtoseconds) with the temperature of the thermostat set to 300 K. Finally, we generate a tight binding model for the system by using maximally localized Wannier functions which were obtained using Wannier90[42,43] and then passed onto the WannierTools code[44] wherein the $\mathbb{Z}_2$ classification was performed around the Wannier charge centers, followed by plotting the surface and edge states using the iterative Green's function method.

3 Results and discussion

3.1 Structural properties

We begin with the structural description of the bulk HH AgSrBi which is predicted to exhibit a face-centered cubic (FCC) structure governed by the $F\bar{4}3m$ [216] space group (as shown in Fig. 1(a)) with the primitive cell vectors defined in terms of the Wyckoff positions of Ag, Sr and Bi as $v_1 = (a/2)(-1, 0, 1)$, $v_2 = (a/2)(0, 1, 1)$ and $v_3 = (a/2)(-1, 1, 0)$, respectively. Based on convergence tests, the optimized lattice constant of $a = 7.31$ Å indicates the global minima/ground state of the system, with bond lengths $d_{Ag–Sr} = 3.65$ Å, $d_{Sr–Bi} = 3.16$ Å and $d_{Ag–Bi} = 3.16$ Å. This structural phase of AgSrBi exhibits a semi-metallic nature which is unusual (since the properties due to pnictogen substitution at site C in the ABC HH should be similar) as compared to AgSrAs which is semi-conducting. This structure is found to be thermally stable since the formation energy is -0.52 eV per atom which implies that the system will form spontaneously when appropriate precursors are combined.

On lowering the crystal symmetry from FCC to hexagonal symmetry (by cleaving the [111] crystal plane (Fig. 1(b)) of the bulk as illustrated in Fig. 1(c)) and confining the system along the [001] crystal direction (by introducing a vacuum of 25 Å), we obtain a crystal structure similar to that of $1T$-MoS_2 (as shown in Fig. 1(c)). This low dimensional phase of AgSrBi has an optimized lattice constant of $a = 4.28$ Å (Fig. 1(c)). The atomic
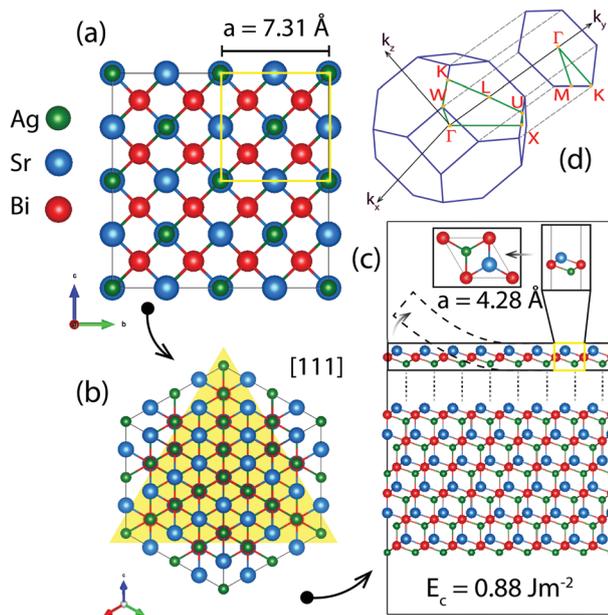
Fig. 1 (a) Face centred cubic (FCC) super-structure of HH AgSrBi (unit cell highlighted in yellow) in which Ag, Sr and Bi are denoted by green, blue and red colors, respectively. (b) The [111] crystal plane of HH AgSrBi which will be cleaved to realise 2D AgSrBi is highlighted in yellow. (c) Schematics of the 1T-MoS$_2$ type structure of the cleaved [111] slab of AgSrBi (with a cleave energy of E_c = 0.88 J m^{-2}), with the unit cell of the monolayer (side and top views) highlighted in yellow. (d) First irreducible BZ of the bulk AgSrBi and the projected hexagonal BZ of low dimensional AgSrBi.

arrangement is of the sandwich type similar to 1T-MoS$_2$ with Ag and Sr atoms occupying the top and bottom layers and the Bi atoms occupying the middle layer as presented in Fig. 1(c). This structure is governed by the $P\bar{3}m1$ [164] space group. The height (t) of this sandwich-type structure is 2.11 Å with interatomic distances $d_{\text{Ag–Sr}}$, $d_{\text{Ag–Bi}}$ and $d_{\text{Sr–Bi}}$ of 3.65 Å, 3.16 Å and 3.16 Å, respectively. The cohesive energy of this system is −6.94 eV per atom, which is comparable to that of graphene,[45] indicating exfoliation from the [111] crystal plane as a potential route to experimentally realising the system other than techniques such as molecular beam epitaxy.

3.2 Dynamic and structural stability

Since there is a lack of experimental and theoretical data on the vibrational modes of AgSrBi, we proceed with the investigation of phonon modes which would give insights into the lattice dynamics and stability. It is evident from Fig. 2(a) that AgSrBi does not exhibit any negative/imaginary frequency in the BZ (presented in Fig. 1(d)), indicating the dynamical stability of AgSrBi under pristine conditions in the harmonic approximation regime. There are a total of nine phonon branches with three acoustic and six optical phonon branches due to the three atoms in the primitive cell. The lower frequency regime is governed by heavier Ag and Bi atoms, whereas the higher frequency regime is governed by the lighter Sr atoms with slight contributions from the Ag atoms. At zero pressure which corresponds to the pristine conditions, the acoustic branches
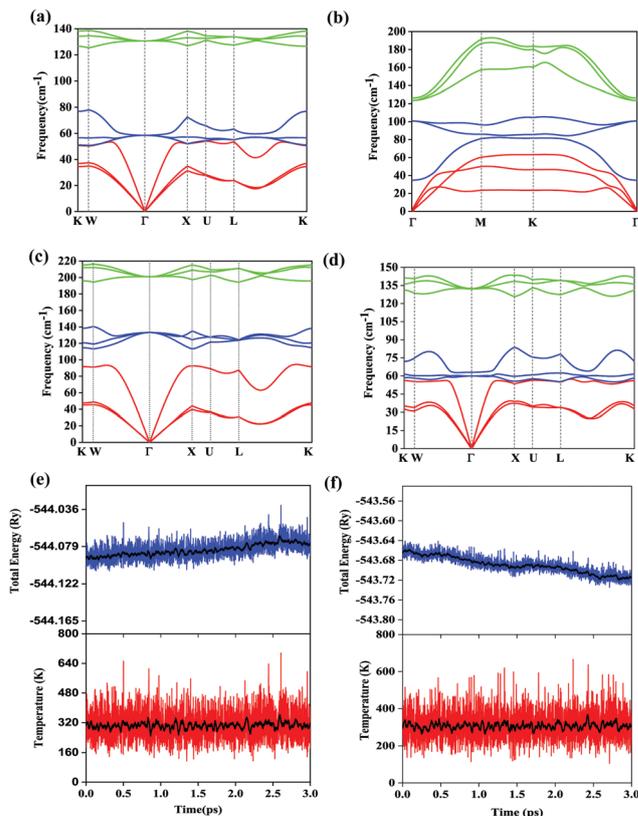

Fig. 2 Phonon dispersion curves of (a) bulk FCC AgSrBi, (b) [111] phase of AgSrBi, (c) bulk FCC AgSrBi at 10% isotropic strain (∼23.5 GPa VCP) and (d) bulk FCC AgSrBi at 1.3% uniaxial strain (broken cubic symmetry). (e–f) AIMD plots of the total energy (Ry) *vs.* time (ps) and temperature (K) *vs.* time (ps) for the bulk and low dimensional phase of AgSrBi, respectively, for a time step of 3 picoseconds (3000 femtoseconds) at a thermostat temperature of 300 K.

lie around 50–60, and this implies that AgSrBi would exhibit an isotropically low thermal conductivity (κ) which is a key factor from the thermoelectric perspective (since κ depends quadratically on the slope of the acoustic branches). Also, since all the branches at zero pressure lie below 200 cm^{-1}, we can also expect the system to be stable at higher temperatures owing to the vibrational entropy. Apart from this, a peculiar feature at zero pressure is the degeneracy and mixing of the acoustic and optical phonon branches, which indicates the semi-metallic behaviour of the material and the similarity of the system with rock-salt oxides. The degenerate longitudinal optical (LO) and transverse optical (TO) branches at the zone center Γ indicate the absence of long range dipole–dipole interactions and hence confirm the non-semiconducting character of the system. We scan the phonon dispersion curves by varying the pressure from 0.0 GPa to ∼23.5 GPa and find that the system is dynamically stable throughout as evident from the phonon dispersion curves at 10% strain (∼ 23.5 GPa) presented in Fig. 2(c). However, there is an increase in the softening between L–K points in the BZ which implies that even higher pressures would eventually make the system dynamically unstable. Similarly, the phonon dispersion curves of AgSrBi at 1.3% uniaxial

strain (broken symmetry) and for the [111] phase of AgSrBi are presented in Fig. 2(d) and (b), respectively. It is evident that, in both cases, the system is dynamically stable. Apart from this, from the room temperature application point-of-view, we perform the AIMD simulations (as evident from the plots presented in Fig. 2(e and f)) and find the system to be structurally stable, which further reinforces the stability criteria.

3.3 Electronic properties

3.3.1 Broken cubic symmetry. Under pristine conditions, *i.e.*, in the absence of pressure and SOC, bulk AgSrBi exhibits a semi-metallic band structure with degenerate valence and conduction bands crossing each other at the Fermi level along the high symmetry point Γ in the entire BZ (as evident from Fig. 3(a)). We restrict our investigation of the electronic band structure in the vicinity of the Fermi level since the low energy electronic properties of materials can be determined by the

Fig. 3 (a) Electronic band structure of bulk FCC AgSrBi under 0% strain. (b) Variation of the energy gap with respect to isotropic strain (VCP) indicating a semi-metal to trivial insulator transition. (c) Electronic band structure of the [111] plane of AgSrBi cleaved from the bulk FCC structure.

nature of bands located in this region. From Fig. 4(a), in the presence of SOC it is evident that the valence band maximum has a doubly degenerate state along the high symmetry point Γ, whereas the conduction band minimum has a single non-degenerate state which is protected by the two-fold symmetry of the FCC structure. This is contrary to the typically expected quadratic contact triple point degeneracy which is observed in well-known topological semi-metals with the structural phase similar to that of MgAgAs-type ones but absent in cubic systems such as KNa_2 Bi and in HH compounds such as LaPtBi, YPtBi, and ScPtBi.[46–48] From the partial density of states (presented in Fig. 4(b)) it is clear that the valence band is populated by the -p and -d orbitals of Bi and Ag, respectively, whereas the conduction band is populated by -s and -d orbitals of Ag, -s orbitals of Sr and -s and -p orbitals of Bi. In order to realize TPT, we subject the bulk FCC AgSrBi to isotropic compressive pressure (VCP) and expansive pressure (VEP). On application of VEP the system retained its semi-metallic character, whereas at a higher VCP (10%) the degeneracy is lifted off at Γ in the BZ. However, further investigation suggested that this gap is trivial in nature (above 8% VCP, while the system is semimetallic below 8% VCP) as shown in the energy-gap *vs.* %VCP plot presented in Fig. 3(b). In order to realise the non-trivial nature we break the cubic symmetry by applying uniaxial strain along the [100] crystal direction.

Application of uniaxial compressive strain breaks the cubic symmetry and alters the orbital character. This enhances the SOC effect leading to the non-trivial TI phase. Breaking the cubic symmetry of a system has been one of the effective methods to realize a non-trivial gap (in the otherwise degenerate states), leading to the much desired TI nature.[46,49] When subjecting bulk FCC AgSrBi to uniaxial compressive strain (in steps of 0.1%) along the [100] crystal direction (in the presence of SOC) we observe non-trivial behavior. At 0.2% (1.5 GPa) strain itself the degeneracy at Γ is lifted off, but the conduction band encapsulates the Fermi level, indicating the topological conductor nature.[49] However, on further increasing the strain we arrive at a critical strain of 1.3% (1.9 GPa) which gives rise to a non-trivial gap of 0.35 meV with the Fermi level lying in between the conduction and valence bands (presented in Fig. 4(c)). This gap is global in nature and retained throughout the BZ, indicating the possibility of low-dimensional conducting surface states. The band inversion mechanism behind this non-trivial gap is due to the increase in -d and -p orbital contributions in the valence band (presented in Fig. 4(d)) from Ag and Bi, respectively, whereas the -s and -p, -s, and -s and -d orbital contributions from Bi, Sr, and Ag, respectively, increase in the conduction band as evident from Fig. 4(d). This makes it clear that the band inversion is quite unconventional (due to the involvement of the three orbitals -s, -p and -d) as compared to typical -s–p orbital inversion which is commonly observed in most of the HH compounds.

3.3.2 Lowering crystal symmetry and dimensional confinement. Another route to realize non-trivial topological behavior in materials is by lowering the crystal symmetry and confining the system in a particular crystal direction. This method has
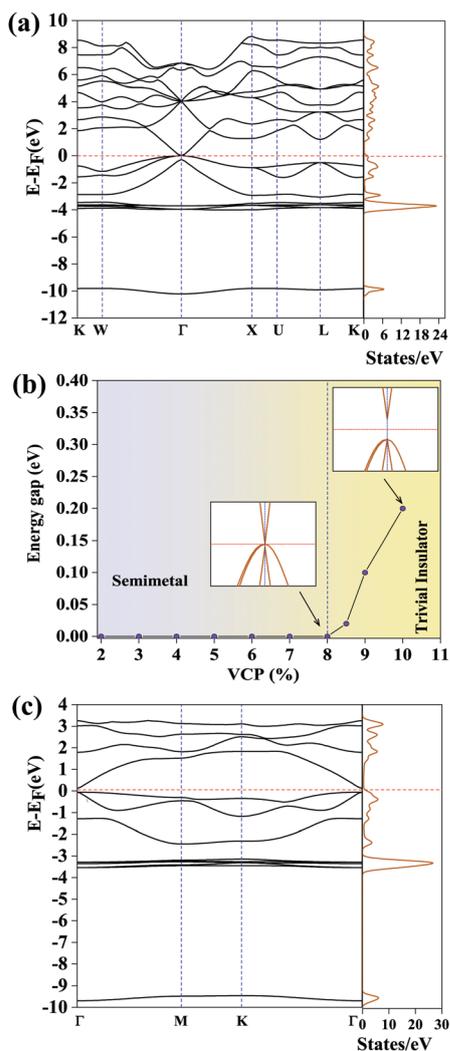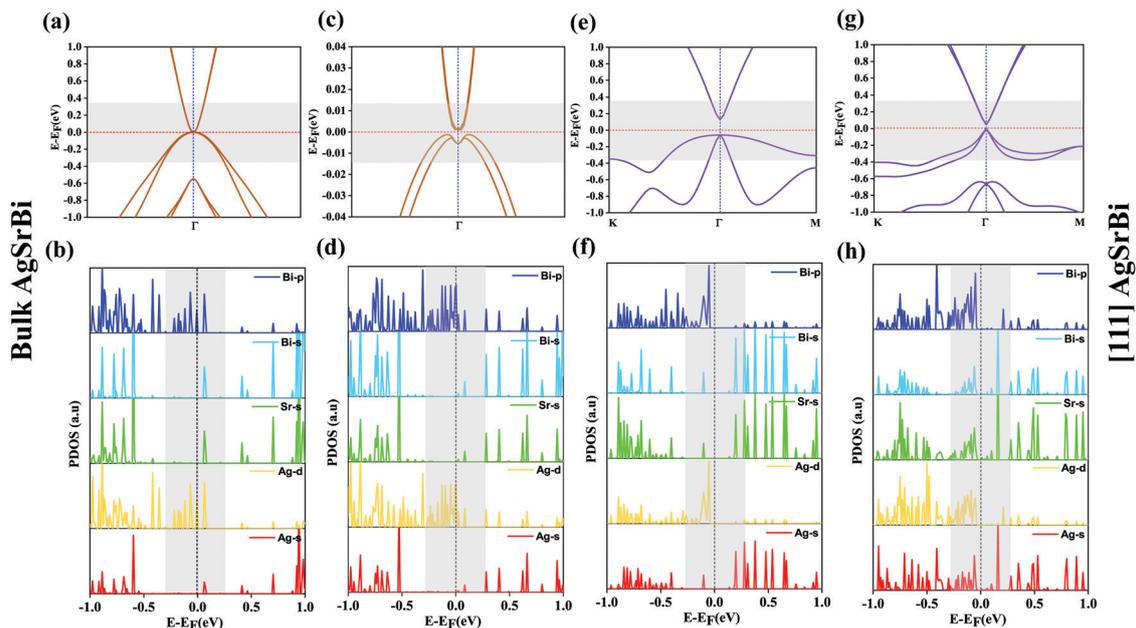
Fig. 4 Electronic band structure and orbital projected density of states of bulk FCC AgSrBi with SOC at (a and b) 0% and (c and d) 1.3%, and the [111] plane of AgSrBi (e and f) without and (g and h) with SOC.

been previously explored in the HgTe binary compound.[50] The bulk phase (with cubic symmetry) of HgTe does not exhibit the topological character, whereas on lowering the crystal symmetry (to a hexagonal symmetry) and confining the system in one dimension gives rise to interesting topological properties. The lower crystal symmetry was achieved by cleaving the [111] plane of the bulk HgTe compound and confining it along the [001] crystal direction. This opened the gap in the degenerate electronic structure (as compared to bulk), but the band ordering was trivial. The band ordering was then fine-tuned by designing quantum wells of CdTe and HgTe with the thickness of the quantum wells governing the critical regime of the system which would enable the non-trivial topology characterized by the inverted band order.

In the case of AgSrBi, we expect the nature of the electronic structure to be analogous to low dimensional HgTe which as compared to its bulk phase exhibits TI nature. For this purpose, we reduce the crystal symmetry of bulk AgSrBi and confine the resulting system into one dimension along the [001] crystal direction. This can be done by cleaving the system from the [111] slab of the bulk as illustrated in Fig. 1(c). The required cleave energy E_c is calculated (using the formula mentioned by Wang *et al.*) to be $E_c = 0.88$ J m^{-2}.[51] Similar to HgTe, the low dimensional phase of AgSrBi exhibits a semi-conducting nature with a global gap of 0.19 eV along the high symmetry point Γ in the BZ (as evident from Fig. 3(c) and 4(e)). In the absence of external stress on the system, we impose SOC effects into our calculations and find that the gap is reduced to 39 meV along the high symmetry point Γ in the BZ (as evident from Fig. 4(g)). This gap is non-trivial in nature and superior to some previously reported systems.[52,53] However, this gap can be further enhanced by subjecting the system to strain, functionalization

(partial/complete) and by creating a multilayer system.[54,55] The non-trivial nature of the gap is clearly evident from the projected density of states presented in Fig. 4(f and h). In the absence of SOC (Fig. 4(f)), the valence band maximum is dominated by -p and -d orbital contributions from Bi and Ag, respectively, with minor contributions arising from the -s orbitals of Ag, Sr and Bi, whereas the conduction band minimum is dominated purely by the -s orbitals of Ag, Sr and Bi, while the contributions from the -p and -d orbitals of Bi and Ag, respectively, are absent (as evident from Fig. 4(f)).

On imposing SOC, a clear band inversion is observed as evident from Fig. 4(h). Due to SOC, the -p and -d orbital contributions from Bi and Ag, respectively, become prominent in the conduction band minimum (Fig. 4(h)), whereas, in the valence band maximum, the contributions from the -s orbitals of Ag, Sr and Bi become prominent which were previously almost negligible (as evident from Fig. 4(h)). We attribute such non-trivial phenomena to the quantum confinement effects and the extra degrees of freedom to electrons owing to the vacuum along the [001] direction. In order to confirm the non-trivial topological character, we further classify the proposed systems as belonging to the $\mathbb{Z}_2$ topological class, followed by computing the surface state (SS) and edge state (ES) spectra using the iterative Green's function method.

3.4 $\mathbb{Z}_2$ analysis and surface/edge state spectra

The non-trivial topology of materials is classified in terms of the $\mathbb{Z}_2$ invariant. Typically, the $\mathbb{Z}_2$ invariants for materials with inversion symmetry are calculated as the product of parities of eigenvalues at time reversal invariant momentum (TRIM) points. However, since HH compounds like AgSrBi do not possess inversion symmetry (owing to the cubic crystal
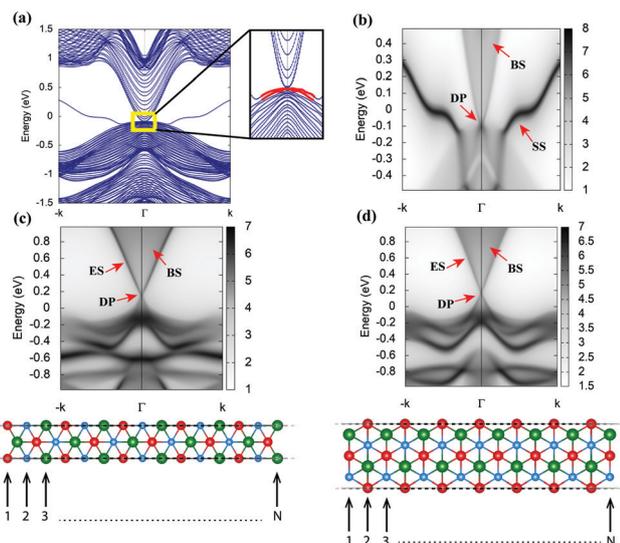
Fig. 5 (a) Slab band structure of bulk AgSrBi at 1.3% uniaxial strain indicating conducting SS (with DP highlighted in red). (b) ARPES-like SS spectrum of bulk AgSrBi at 1.3% uniaxial strain with bulk states (BS) and DP clearly evident. (c and d) ARPES-like ES spectra of the zig-zag edge (structure below (c)) and planar edge (structure below (d)) configurations with a ribbon width index N = 15 of the AgSrBi nanoribbon, indicating the presence of DP and insulating BS.

structure), the $\mathbb{Z}_2$ invariant is computed along two different momentum planes in the BZ, *i.e.*, $(\mathbb{Z}_2)_{(k=\pi)}$ and $(\mathbb{Z}_2)_{(k=0)}$. These calculations are done in terms of the Wannier charge center in the vicinity of the Fermi level using the WannierTools code which utilizes the tight binding model obtained from the Wannier functions using the Wannier90 code. The $\mathbb{Z}_2$ invariants for bulk systems are calculated along six time reversal invariant planes (TRIP) *i.e.*, $k_x = 0$, π, $k_y = 0$, π and $k = 0$, π in the BZ. At a critical uniaxial strain of 1.3% (1.9 GPa) which corresponds to the non-trivial gap in the bulk AgSrBi (presented in Fig. 4(c)), we compute the $\mathbb{Z}_2$ invariants using eqn (1) and (2), and find them to be $(\nu_0, \nu_1\nu_2\nu_3) = (1, 101)$. This indicates the strong topological insulating nature of bulk AgSrBi.

$$\nu_0 = (\mathbb{Z}_2(k_{i=0}) + \mathbb{Z}_2(k_{i=0.5}))\mathrm{mod}2 \quad (1)$$

$$\nu_i = \mathbb{Z}_2(k_{i=0.5}) \quad (2)$$

The corresponding slab band structure indicating SS and ARPES like SS spectra are computed using the iterative Green's function method along the [111] crystal direction and shown in Fig. 5(a and b). This shows clearly that the bulk gap in AgSrBi at critical uniaxial strain enables the non-trivial Dirac point (DP) along the high symmetry point in the BZ and SS which are robust against external perturbations (presented in Fig. 5(b)). Similarly, the non-trivial nature of the lower crystal symmetry and dimensionally confined system of [111] AgSrBi is characterized by the $\mathbb{Z}_2$ invariant as $\nu = 1$ indicating the non-trivial topological nature with potential applications in spintronic devices. From the ARPES like ES spectra computed for the zig-zag edge and planar edge nanoribbon configurations (for a ribbon width index of N = 15 presented in Fig. 5(c and d)) the

DP is clearly evident, confirming the conducting character of the edges.

4 Conclusion

To sum up, we employ first-principles calculations based on DFT to investigate the TI character of the dynamically and structurally stable HH compound AgSrBi. Under pristine conditions (zero pressure) AgSrBi exhibits semimetallic behavior which is retained even when SOC is considered. However, when subjected to high isotropic compressive pressures ($\sim$23.5 GPa) the system undergoes a quantum phase transition from semimetallic to a trivial insulator. In order to realize the non-trivial nature, we break the cubic crystal symmetry which gives rise to band inversion induced TI nature. This TI nature gives rise to a conducting SS along the [111] direction as evident from the ARPES like SS spectrum, while the bulk displays a global gap. Due to this non-trivial nature, AgSrBi is classified to be a strong TI with $\mathbb{Z}_2$ invariants (1, 101). Similarly, on lowering the crystal symmetry and confining the system along one dimension in the [001] crystal direction, analogous to HgTe, we observe a nontrivial TI nature characterized by the band inversion, $\mathbb{Z}_2$ invariant ($\nu = 1$) and conducting ES spectra. With these results, we propose a potential TI and quantum spin Hall insulator with spintronic degrees of freedom to the electrons and potential nanoelectronic and thermoelectric applications.

Author contributions

BRD & RMS – conceptualization, data curation, formal analysis, investigation, validation, visualization, writing – original draft. PKJ, DK & BC – project administration, resources, supervision, validation, writing – review & editing.

Conflicts of interest

The authors declare that there have no conflicts to declare.

Acknowledgements

References

1 B. A. Bernevig and S.-C. Zhang, *Phys. Rev. Lett.*, 2006, **96**, 106802.
2 M. Z. Hasan and C. L. Kane, *Rev. Mod. Phys.*, 2010, **82**, 3045.
3 N. Armitage, E. Mele and A. Vishwanath, *Rev. Mod. Phys.*, 2018, **90**, 015001.
4 S. M. Young, S. Zaheer, J. C. Teo, C. L. Kane, E. J. Mele and A. M. Rappe, *Phys. Rev. Lett.*, 2012, **108**, 140405.

5 B. Lv, H. Weng, B. Fu, X. P. Wang, H. Miao, J. Ma, P. Richard, X. Huang, L. Zhao and G. Chen, *et al.*, *Phys. Rev. X*, 2015, **5**, 031013.

6 M. M. Hosen, K. Dimitri, I. Belopolski, P. Maldonado, R. Sankar, N. Dhakal, G. Dhakal, T. Cole, P. M. Oppeneer and D. Kaczorowski, *et al.*, *Phys. Rev. B*, 2017, **95**, 161101.

7 A. Burkov, M. Hook and L. Balents, *Phys. Rev. B: Condens. Matter Mater. Phys.*, 2011, **84**, 235126.

8 H. Shi, D. Parker, M.-H. Du and D. J. Singh, *Phys. Rev. Appl.*, 2015, **3**, 014004.

9 X.-L. Qi and S.-C. Zhang, *Rev. Mod. Phys.*, 2011, **83**, 1057.

10 X.-L. Qi, T. L. Hughes and S.-C. Zhang, *Phys. Rev. B: Condens. Matter Mater. Phys.*, 2010, **82**, 184516.

11 F. Völklein and E. Kessler, *Thin Solid Films*, 1987, **155**, 197–208.

12 L. Fu and C. L. Kane, *Phys. Rev. B: Condens. Matter Mater. Phys.*, 2007, **76**, 045302.

13 H. Zhang, C.-X. Liu, X.-L. Qi, X. Dai, Z. Fang and S.-C. Zhang, *Nat. Phys.*, 2009, **5**, 438–442.

14 R. M. Sattigeri, S. B. Pillai, P. K. Jha and B. Chakraborty, *Phys. Chem. Chem. Phys.*, 2020, **22**, 4602–4609.

15 B. Monserrat, J. W. Bennett, K. M. Rabe and D. Vanderbilt, *Phys. Rev. Lett.*, 2017, **119**, 036802.

16 M. K. Yadav and B. Sanyal, *J. Alloys Compd.*, 2015, **622**, 388–393.

17 A. Roy, J. W. Bennett, K. M. Rabe and D. Vanderbilt, *Phys. Rev. Lett.*, 2012, **109**, 037602.

18 K. Gofryk, D. Kaczorowski, T. Plackowski, J. Mucha, A. Leithe-Jasper, W. Schnelle and Y. Grin, *Phys. Rev. B: Condens. Matter Mater. Phys.*, 2007, **75**, 224426.

19 C. Timm, A. Schnyder, D. Agterberg and P. Brydon, *Phys. Rev. B*, 2017, **96**, 094526.

20 Y. Pan, A. Nikitin, T. Bay, Y. Huang, C. Paulsen, B. Yan and A. De Visser, *EPL*, 2013, **104**, 27001.

21 S. Populoh, M. Aguirre, O. Brunko, K. Galazka, Y. Lu and A. Weidenkaff, *Scr. Mater.*, 2012, **66**, 1073–1076.

22 X. Zhang, L. Yu, A. Zakutayev and A. Zunger, *Adv. Funct. Mater.*, 2012, **22**, 1425–1435.

23 A. Bansil, H. Lin and T. Das, *Rev. Mod. Phys.*, 2016, **88**, 021004.

24 P.-J. Guo, H.-C. Yang, K. Liu and Z.-Y. Lu, *Phys. Rev. B*, 2017, **96**, 081112.

25 J.-Y. You, X.-J. Dong, B. Gu and G. Su, *Phys. Rev. B*, 2021, **103**, 104403.

26 K.-H. Jin, H. W. Yeom and F. Liu, *Phys. Rev. B*, 2020, **101**, 035111.

27 H. Yao, C. Chen, W. Xue, F. Bai, F. Cao, Y. Lan, X. Liu, Y. Wang, D. J. Singh and X. Lin, *et al.*, *Sci. Adv.*, 2021, **7**, eabd6162.

28 R. M. Sattigeri and P. K. Jha, *Sci. Rep.*, 2021, **11**, 1–10.

29 L. Winterfeld, L. A. Agapito, J. Li, N. Kioussis, P. Blaha and Y. P. Chen, *Phys. Rev. B: Condens. Matter Mater. Phys.*, 2013, **87**, 075143.

30 B. Bradlyn, L. Elcoro, J. Cano, M. Vergniory, Z. Wang, C. Felser, M. I. Aroyo and B. A. Bernevig, *Nature*, 2017, **547**, 298–305.

31 M. Vergniory, L. Elcoro, C. Felser, N. Regnault, B. A. Bernevig and Z. Wang, *Nature*, 2019, **566**, 480–485.

32 W. Feng, W. Zhu, H. H. Weitering, G. M. Stocks, Y. Yao and D. Xiao, *Phys. Rev. B: Condens. Matter Mater. Phys.*, 2012, **85**, 195114.

33 I. Zeljkovic, Y. Okada, M. Serbyn, R. Sankar, D. Walkup, W. Zhou, J. Liu, G. Chang, Y. J. Wang and M. Z. Hasan, *et al.*, *Nat. Mater.*, 2015, **14**, 318–324.

34 F. Wei, C.-W. Liu, D. Li, C.-Y. Wang, H.-R. Zhang, J.-R. Sun, X. P. Gao, S. Ma and Z. Zhang, *Phys. Rev. B*, 2018, **98**, 161301.

35 J. Seidel, *Nat. Mater.*, 2019, **18**, 188–190.

36 M. He, H. Sun and Q. L. He, *Front. Phys.*, 2019, **14**, 43401.

37 P. Giannozzi, O. Andreussi, T. Brumme, O. Bunau, M. B. Nardelli, M. Calandra, R. Car, C. Cavazzoni, D. Ceresoli and M. Cococcioni, *et al.*, *J. Phys.: Condens. Matter*, 2017, **29**, 465901.

38 N. Troullier and J. L. Martins, *Phys. Rev. B: Condens. Matter Mater. Phys.*, 1991, **43**, 1993.

39 J. P. Perdew, K. Burke and M. Ernzerhof, *Phys. Rev. Lett.*, 1996, **77**, 3865.

40 H. J. Monkhorst and J. D. Pack, *Phys. Rev. B: Solid State*, 1976, **13**, 5188.

41 S. Baroni, S. De Gironcoli, A. Dal Corso and P. Giannozzi, *Rev. Mod. Phys.*, 2001, **73**, 515.

42 N. Marzari, A. A. Mostofi, J. R. Yates, I. Souza and D. Vanderbilt, *Rev. Mod. Phys.*, 2012, **84**, 1419.

43 A. A. Mostofi, J. R. Yates, Y.-S. Lee, I. Souza, D. Vanderbilt and N. Marzari, *Comput. Phys. Commun.*, 2008, **178**, 685–699.

44 Q. Wu, S. Zhang, H.-F. Song, M. Troyer and A. A. Soluyanov, *Comput. Phys. Commun.*, 2018, **224**, 405–416.

45 J. Zhao, J.-W. Jiang, Y. Jia, W. Guo and T. Rabczuk, *Carbon*, 2013, **57**, 108–119.

46 I. Y. Sklyadneva, I. P. Rusinov, R. Heid, K.-P. Bohnen, P. M. Echenique and E. V. Chulkov, *Sci. Rep.*, 2016, **6**, 1–9.

47 W. Al-Sawai, H. Lin, R. Markiewicz, L. Wray, Y. Xia, S.-Y. Xu, M. Hasan and A. Bansil, *Phys. Rev. B: Condens. Matter Mater. Phys.*, 2010, **82**, 125208.

48 D. Xiao, Y. Yao, W. Feng, J. Wen, W. Zhu, X.-Q. Chen, G. M. Stocks and Z. Zhang, *Phys. Rev. Lett.*, 2010, **105**, 096404.

49 R. M. Sattigeri, T. K. Gajaria, P. K. Jha, P. Śpiewak and K. J. Kurzydłowski, *J. Phys.: Condens. Matter*, 2021, **33**, 155402.

50 J. Li, C. He, L. Meng, H. Xiao, C. Tang, X. Wei, J. Kim, N. Kioussis, G. M. Stocks and J. Zhong, *Sci. Rep.*, 2015, **5**, 1–9.

51 L. Wang, K. C. Lai, L. Huang, J. W. Evans and Y. Han, *Surf. Sci.*, 2020, **695**, 121532.

52 Y. Ma, L. Kou, Y. Dai and T. Heine, *Phys. Rev. B*, 2016, **94**, 201104.

53 X.-L. Sheng, C. Chen, H. Liu, Z. Chen, Z.-M. Yu, Y. Zhao and S. A. Yang, *Phys. Rev. Lett.*, 2019, **123**, 256402.

54 H. Weng, A. Ranjbar, Y. Liang, Z. Song, M. Khazaei, S. Yunoki, M. Arai, Y. Kawazoe, Z. Fang and X. Dai, *Phys. Rev. B: Condens. Matter Mater. Phys.*, 2015, **92**, 075436.

55 S. Zhang, W. Zhou, Y. Ma, J. Ji, B. Cai, S. A. Yang, Z. Zhu, Z. Chen and H. Zeng, *Nano Lett.*, 2017, **17**, 3434–3440.